Searching for Long Period Variables in Globular Clusters: A Demonstration on NGC 1851 using PROMPT

Andrew C. Layden, Andrew J. Broderick

Physics & Astronomy Department, Bowling Green State University, Bowling Green, OH 43403

B. L. Pohl, D. E. Reichart, K. M. Ivarsen, J. B. Haislip, M. C. Nysewander, A. P. LaCluyze

Department of Physics & Astronomy, University of North Carolina, Chapel Hill, NC, 27599

and

T. M. Corwin

Department of Physics & Astronomy, University of North Carolina, Charlotte, NC 28223

ABSTRACT

We demonstrate how a small, robotically-controlled telescope can be used to monitor bright, long-period variable stars in dense stellar systems like Galactic globular clusters. Observations of NGC 1851 gathered with the #5 PROMPT 0.4-m telescope in $BVRI$ yielded quality color-magnitude diagrams to well below the horizontal branch at $V = 16.1$ mag. We recovered many of the known RR Lyrae variables, clarified the nature of the three known bright variables in the cluster, detected two new long period variables, and flagged seven more suspected variables. We describe methods that should yield good results in variable star searches and monitoring using this and other small telescopes.

Subject headings: variable stars: general — globular clusters: individual (NGC 1851)

1. Introduction

Variable stars provide important constraints on models of stellar structure, evolution, and pulsation. Variable stars in globular clusters are particularly valuable since these systems

have little internal spread in composition, age, or line-of-sight distance, thereby controlling many important parameters. Long period variable stars (LPVs) in globular clusters were studied extensively in the optical up through the 1970's using photographic plates (e.g., see the review by Feast (1973)), but little work has been done using CCDs and digital photometric analysis apart from the study of 47 Tucanae by Lebzelter & Wood (2005). Clement et al. (2001) note that, "These types of stars have not been well surveyed in the Galactic globular clusters because most search programs are designed to optimize detection and period determination for variables with periods less than one day. Thus our sample is probably incomplete." Looking at existing finder charts for cluster LPVs, one notices that the crowded cluster centers tend to be under-represented, in part because so much of the existing survey work was done photographically. A new survey of LPVs in globular clusters is clearly warranted given improvements in CCD detectors and digital photometric methods.

The advent of robotically-controlled telescopes like those of the Panchromatic Robotic Optical Monitoring and Polarimetry Telescopes (PROMPT) (Reichart et al. 2005) facilitate the acquisition of a few images a week over a span of years. To demonstrate the feasibility of observing LPVs with PROMPT, we selected the globular cluster NGC 1851.

This cluster is typical of the angular diameter and horizontal branch magnitude of the clusters we plan to monitor, and it was well-placed on the sky during the time of our study. The central concentration of NGC 1851 ($c = 2.32$, Harris (1996)) is higher than average, making it a more challenging target than most in terms of photometric crowding. Its high latitude and low reddening, $b = +35°$ and $E(B-V) = 0.02$ mag (Harris 1996), make it a good test of PROMPT's photometric capability, since the principle sequences in the CMD should be intrinsically narrow. Furthermore, NGC 1851 has a well-studied variable star population including a plethora of RR Lyrae variables (Bailey 1924; Fourcade & Laborde 1966; Liller 1975; Wehlau et al. 1978; Stetson 1981; Wehlau et al. 1982; Walker 1998; Downes et al. 2004; Sumerel et al. 2004) and three bright suspected variables : V2, V9 and V24 (Clement et al. 2001).

In this paper, we describe our observations and reductions in Sec. 2, present our point spread function photometry in Sec. 3, and discuss our search for stellar variability and the resulting light curves in Sec. 4. We summarize our results in Sec. 5 and comment on the utility of the PROMPT telescopes as a means for monitoring long period variable stars in other globular clusters.

2. Observations and Reductions

We acquired images of NGC 1851 through $BVRI$ filters on ten nights between 2006 December 04 and 2007 May 14 using PROMPT 5, a 0.4-m R-C telescope with an Alta U47+s CCD camera by Apogee (Reichart et al. 2005). This system gives images with a 0.58 arcsec pix^{-1} scale and $\sim$10 arcmin field of view. The telescope does not use an active guiding system, and we found that exposures longer than $\sim$80 sec tended to trail. After some experimentation, we found the following sequence to be a good compromise between depth and image quality: four 80 sec exposures in V and in R, five 80 sec exposures in B, and four 40 sec exposures in I. The shorter exposure times in I ensured that the bright LPVs did not saturate during times of good seeing. The images in a specific filter were combined as described below to achieve the desired depth. By interleaving the image sequence (e.g., ordering the sequence $BVRI, BVRI, BVRI, BVRI, B$ rather than $BBBBB, VVVV, RRRR, IIII$), the slight tracking drift of the telescope tended to shift stars across any bad pixels.

The web-based SKYNET client[1] allowed us to request and retrieve images remotely via the internet. It also provided nightly calibration images including bias, dark, and flat-field images. We processed the cluster images using standard methods. The individual cluster images in a given filter were then averaged using a bad-pixel rejection algorithm to provide a single, deep, high signal-to-noise image for each filter per night; an image which is largely free of blemishes due to cosmic rays or hot/bad pixels. If one or more of the images suffered from trailing, poor focus or seeing, or intermittent clouds, it could be removed from the averaging process. On nights when the sky background varied by more than 10%, we added a constant to each image to bring all images to a consistent sky level before coadding them. The act of combining the individual images greatly reduced the number of images in the time series, making the photometric analysis faster and simpler. The fwhm of the stellar profiles on the combined images ranged from 1.6 to 4.3 arcsec, with a median seeing of 2.4 arcsec.

3. DAOPHOT Photometry

We analyzed the resulting images using the DAOPHOT II point-spread function (PSF) fitting photometry package (Stetson 1987) following the procedure outlined therein. We selected up to 150 PSF stars distributed across each image while avoiding the crowded cluster center. We built and iteratively improved the PSF model by fitting and removing

---

[1]See http://skynet.unc.edu.

faint neighboring stars, and then used ALLSTAR to obtain optimal photometry for the sources detected on the image. An additional application of DAOPHOT/ALLSTAR to the subtracted image found additional faint sources, and ALLSTAR was rerun on the combined source list, resulting in a list for each image containing positions and preliminary PSF photometry of all the objects brighter than $\sim 3\sigma$ above the background level.

Because the background level and seeing varied considerably from one image to the next, the number of stars detected varied greatly. To generate a more uniform star list, we combined the 11 best-quality VRI images using MONTAGE to produce a master image[2] with very high signal-to-noise. The DAOPHOT/ALLSTAR procedure described above was applied to this image, yielding a master list of stellar sources in our field.

The ALLSTAR source coordinates from the individual frames were matched using DAO-MASTER, and ALLFRAME (Stetson 1994) was run on all the images simultaneously using the master list of stellar positions from the MONTAGE image. The resulting photometry files were combined in filter-specific sets using DAOMASTER. This provided both averaged and time-series photometry for each source in the master list on an instrumental magnitude system, $bvri$.

Stetson (2000) provides high-quality photometric standard stars in the field of NGC 1851 in BVI. We selected over 60 bright standards spanning a range of colors and identified them in our averaged $bvri$ photometry file. We then performed least-squares fits to determine the coefficients $c_{0,f}$ and $c_{1,f}$ that would allow us to transform all our instrumental photometry onto the Stetson standard system:

$$b - B = c_{0,B} + c_{1,B}(B - V), \quad v - V = c_{0,V} + c_{1,V}(V - I), \quad i - I = c_{0,I} + c_{1,I}(V - I).$$

The rms of the points about each of these fits was 0.024, 0.016, and 0.019 mag, respectively. The color terms were $c_{1,f} = -0.191$, 0.013, and -0.055 respectively. Thus the PROMPT filters and CCD combination transform well to the standard system in V and I, though not so well in B where there was a weak quadratic behavior which we chose not to fit. Plots of residuals as a function of magnitude, X-, and Y-position showed no significant trends, giving us confidence that our calibration is sound.

Stetson (2000) did not provide R magnitudes for his standard stars in NGC 1851, and we were unable to locate other high-quality R-band photometry in the literature, so we provide

---

[2]Available at `http://physics.bgsu.edu/~layden/publ.htm` along with other data products from this study.

the following provisional calibration of our r photometry. To get a general conversion from V to R, we used Stetson's VRI standard stars in NGC 5904 to fit $R' = V + a_0 + a_1(V - I)$, obtaining $a_0 = 0.0459$ and $a_1 = -0.524$ with rms $= 0.016$ mag. We then computed R' for each of our Stetson standards in NGC 1851 from his V and $V - I$ values, and compared them to our instrumental r magnitudes via a fit of the form $r - R' = b_0 + b_1(V - I)$, where $b_0 = -0.851$ and $b_1 = 0.0165$. The rms of 0.013 mag gives us confidence that our R' magnitudes are reliable internally, but there may be systematic errors, so we consider the R' magnitudes provisional.

Figure 1 shows color magnitude diagrams drawn from this data for various passband combinations. To reduce the effects of crowding, we plot only stars with projected radii larger than 1.0 arcmin from the cluster center. The $(B - V, B)$ CMD has more scatter than the others, consistent with the lower throughput of the PROMPT5 filter/CCD system in B. The other three CMDs show well-defined giant and horizontal branches down to a magnitude or more below the horizontal branch (HB). The bimodal color distribution of the HB described by Stetson (1981) and others is clearly evident. The broader wavelength baseline of $(V - I)$ provides a wider range of colors, and hence better signal-to-noise compared with $(V - R')$.

4.   Variable Star Detection

We used two complementary methods to search for stellar variability in our images. The first was to find stars with unusually large variations in the DAOPHOT $bvri$ time series. The second used the ISIS2.2 image subtraction software of Alard (2000). The former yields light curves in magnitudes on a standard photometric system, but it can be incomplete in the crowded cluster center where photometric errors are large and blending can lead to false-positive detections. The latter method is much less affected by crowding, enabling us to extend the census of variables closer to the cluster center, but the results appear as flux variations which can be difficult to convert to magnitudes in cases when the star's reference magnitude can not be reliably determined (see Zorotovic et al. (2010)).

4.1.   DAOPHOT Magnitudes

We used the variability index, Λ, computed with DAOMASTER to select variable star candidates. DAOMASTER was used to compile the time-series photometry in each filter separately, yielding four independent estimates of stellar variability, $\Lambda_B, \Lambda_V, \Lambda_R$, and Λ_I. We found that blue variables like RR Lyrae stars tended to show up strongly in Λ_B and Λ_V,

owing to their larger amplitudes in these bluer passbands and their better contrast against the background of red subgiant and giant stars. Red variables like LPVs tended to show up well in all passbands.

The panels immediately to the right of each CMD in Figure 1 show Λ on the abscissa as a function of the corresponding stellar magnitude on the ordinate. The large number of low Λ values denote the locus of non-variable stars, and stars that deviate from this locus are variable star candidates. In all four panels, candidates fall at the level of the HB (probably RRL) and the upper RGB (likely LPVs). Stars that have large Λ in multiple filters are especially robust candidates.

For each of the LPV candidates, we extracted the instrumental time-series photometry, along with that of 7-10 nearby comparison stars having low values of Λ, red colors, and low-crowding environments. We computed differential photometry (variable minus comparison) for each comparison star and converted it to a standard magnitude of the variable star using our standard magnitudes of the comparison stars and the photometric transformation coefficients from Section 3. We took the median of these 7-10 estimates as our final estimate of the variable's magnitude on that frame. The results are shown in Table 1, along with the standard error of the mean (ϵ_f) and number of comparison stars (N_f) for each filter. The Julian Date of observation (JD), full-width seeing in arcseconds (FWHM), and airmass (Z) are also recorded. Plotting the photometry as a function of time provides confirmation of a candidate's variability and allows us to characterize the nature of the variability. We also performed this procedure for all stars on the RGB/AGB redder than $V - I = 1.45$ mag to ensure a consistent look at variability with evolutionary state, as well as on several interesting blue stars.

4.2. ISIS Image Subtraction

We used the ISIS2.2 image subtraction software (Alard 2000) to provide a second opinion on variability, particularly near the crowded center of this relatively compact cluster. For simplicity, we restricted the analysis to our V image set and trimmed the images to cover only a 3.5 x 7.6 arcmin region centered on the cluster common to all ten images. Following the procedure outlined in Alard's on-line tutorial,[3] we interpolated the images to remove any shifts and rotations between the images, built a composite reference image out of the best-seeing images, calculated the difference image between this reference and each of the individual images, and detected likely variables from the weighted stack of difference

---

[3]See http://www2.iap.fr/users/alard/tut.html.

images. Frequent and significant rotations between the images in this time-series (due to re-moval of the camera for support and maintenance at this newly-commissioned observatory), along with substantial differences in image quality, made the result noisier than in our past experience with the package, but the results are still useful.

Most of the ISIS detections correspond to known RRL, but several are LPV candidates. In V, the bright, low-amplitude LPVs tended to produce a similar variability signal to the fainter, high-amplitude RRL. Many of the RRL near the cluster center recently studied by Sumerel et al. (2004) are superposed on each other in our moderate seeing images, complicat-ing flux extraction from the ISIS difference images. Some central LPVs may therefore have gone undetected in NGC 1851. We expect this problem will affect us less in the other glob-ulars we aim to survey, since most of them are less centrally-concentrated than NGC 1851 and have fewer RRL.

4.3. Light Curves

The DAOPHOT and ISIS methods detected four bright variable stars, including two pre-viously known variables, V2 and V9 in the catalog of Clement et al. (2001), and two new LPV stars. We also identified seven stars as new suspected variables, and recovered pho-tometry of another previously known LPV, V24, whose variability was below our detection threshold. We do not pursue farther the numerous RRL we detected and cross-referenced with the Clement et al. (2001) catalog, since high quality photometry is already available for these stars from Walker (1998), Sumerel et al. (2004) and others. We now discuss the brighter variables in detail, beginning with the LPV candidates and concluding with two bluer variables with shorter periods.

The variable star candidate with the strongest signal in both the DAOPHOT and ISIS analyses is V9 (our ID#43). Figure 2 shows the light curves for this star. Using the template-fitting method of Layden & Sarajedini (2000), we find the best-fit sine curve to have an amplitude of $A_V = 0.43$ mag and a period of 141 days. However, since our data covers just over one pulsation cycle, we can not say how well these values repeat from cycle to cycle. Liller (1975) found low-level variations in this star, while Wehlau et al. (1978) found this star too blended by neighbors to obtain reliable photographic photometry and suspected it was nonvariable. Our digital imaging proves that this, the reddest star in our data set, is variable, and its light curve and position in the CMD (see Figure 3) indicate it is an LPV. Additional information is listed in Table 2 including equatorial coordinates from the Two Micron All Sky Survey (Strutskie et al. 2006), projected angular radius from the cluster center in arcseconds, mean magnitude and observed magnitude range in each bandpass, and

a comment.

Another very red star is our ID#38. It was not detected in previous variability surveys, but the light curve in Figure 2 indicates it is indeed variable with a period >200 days and amplitude $A_V > 0.5$ mag, and its position in Figure 3 confirms it is an LPV. We designate this star as V54. Note that the seeing and transparency were particularly poor on the eighth night of the time series, resulting in systematically poor photometry for these points on this and all stars' light curves.

In Figure 2, star #29 displays slightly smaller variations which are well-correlated across all four filters. The magnitude range of the variations decays as we move from B to I, as expected for an LPV. Though our sampling cadence is too coarse to resolve clear cyclic behavior or derive the star's period, we are nevertheless confident this star is an LPV, so we designate it as V55.

Another star near the giant branch tip is #22. Its light curve shows evidence of variations that are correlated across V, R', and I, suggesting it is a low-amplitude LPV. The larger uncertainties in B due to crowding may mask the correlation. We detected this star with ISIS but its signature is weaker and is partially blended with surrounding variables. We label this as a suspected variable and encourage further monitoring. Several other stars showed low-level variations similar to that of #22, and we label them as suspected variables as well, and list their properites in Table 2: #33, #34, #7, #14, and #26. Many of these stars lie above the giant branch in Figure 3, consistent with their being LPVs that are blended with other bright, unresolved stars in our DAOPHOT photometry. Blending is an expected consequence of these stars' more central location in the cluster.

We did not detect the other known LPV in the cluster, V24 (#31). Its Λ_f values were below our variability detection thresholds in all four filters, and the star was located outside the region used in our ISIS analysis. Our photometry for this star, presented in the left panel of Figure 4, shows no obvious variability with the 183 day period advocated by Wehlau et al. (1982). The right panel shows the Wehlau et al. (1982) photographic data folded by the 183 day period. A coherent variation with an amplitude of $A_B \approx 0.1$ mag is evident. A skeptic might note that the Wehlau data was acquired during five short observing runs using several different telescopes, and the data from these runs fall at specific phases, so that systematic zero point errors from run to run might be interpreted as stellar variation. However, Stetson (1981) also detected variation in this star (his #168) between two photoelectric photometry runs in 1977 and 1980: $\Delta V = 0.071 \pm 0.013$ and $\Delta B - V = 0.021 \pm 0.014$ mag, and his data phase-up with those of Wehlau in Figure 4, so we conclude that the star is a low-amplitude LPV. We recognize that LPVs with amplitudes under ~ 0.1 mag likely go undetected in our study of NGC 1851. We also note that our mean B CCD photometry is in excellent

agreement with that of Wehlau et al. (1982) and Stetson (1981), despite its larger scatter ($\sigma_B = 0.10$ mag).

The third known variable in NGC 1851 brighter than the HB is V2. It was discovered by Bailey (1924), who suggested its period was "probably short." Liller (1975) found no variability in V2 but noted its proximity to a star of similar brightness. Wehlau et al. (1978) reached similar conclusions. Wehlau et al. (1982) and Walker (1998) did not present photometry for V2. Using ISIS image subtraction, Sumerel et al. (2004) found an RRL star, V51, ∼1.4 arcsec from the published position of V2. In our images, there is a resolved blend at this position, but only the south-eastern of the two stars in the blend (our ID#207) is variable. The variations are consistent with a short period, so we suspect that V2 and V51 refer to the same star. The mean magnitude and color of #207 place it above and redward of the cluster RRL (see Figure 3), suggesting it may be a type II Cepheid member of the cluster. However, the star is a bit redder than the expected location of the instability strip, and of the type II Cepheids listed by Nemec, Nemec, & Lutz (1994). Another possibility is that it is an RRL blended with an unresolved red giant star. To investigate this possibility, we folded our DAOPHOT data with the period for V51 recommended by Sumerel et al. (2004), 0.507 days. The resulting light curve had significant scatter. We performed a period search (Layden & Sarajedini 2000) over 0.3 to 20 days and found good light curves at 0.3373 and 0.5095 day periods with an RRab light curve template. This period search also yielded acceptable light curves at a number of longer periods consistent with an anomalous Cepheid or type II Cepheid. We folded the original ISIS data from Sumerel et al. (2004) by these periods, and successfully ruled out all the longer periods; the best fits were were at 0.340 and 0.510 days (±0.002 days), both made with an RRab template. The former period had a smaller rms scatter around the best-fit template, but is quite short for a fundamental mode pulsator (Castellani et al. 2003), and the RRc template produced poor fits. More observations are required to uniquely determine this star's period, though the period ∼0.5095 days seems most probable. The bright magnitudes and small amplitudes shown in Table 2 are in excellent agreement with expectations for a cluster RRab star in an unresolved blend with a red giant branch star having $V \approx 15.4$ mag. We find this to be the best explanation for star #207.

Finally, we detected one variable, using both DAOPHOT and ISIS, at a location not previously reported. Star #377 is surrounded by several stars of similar brightness. The star is about 0.3 mag brighter than the level of the other RRL (see Figure 3), and a period search over 0.15 to 10 days found only two promising periods, at 0.3434 and 0.5233 days. We suspect this star is an RRL blended with another star.

5.   Conclusions

Our photometry has yielded good CMDs in $BVRI$ for the brighter stellar sequences of NGC 1851, along with time-series data that have helped to clarify the nature of several bright variables in the cluster. Several previous researchers suggested V9 was not variable, whereas our photometry clearly shows V9 to be an LPV with a period of ∼140 days and a V amplitude of ∼0.4 mag. Previous studies have also suggested V2 is not variable; we believe it is the same star as V51 recently observed by Sumerel et al. (2004), and conclude that it is an RRL blended with a red giant star. V24 is a known LPV with amplitude $A_B \approx 0.1$ mag, just below the detection threshold of our time series.

We have detected two new low-amplitude LPVs, ID#38 and #29, designating them V54 and V55, respectively. We also flagged six other bright, red stars as suspected variables, and detected a new variable, ID#377, which appears to be an RRL blended with another star. A more extensive time series is needed to clarify the nature of these stars. Given the high Galactic latitude of NGC 1851 and the small R_{proj} values in Table 2, we expect that all the variables and suspected variables are cluster members.

Figure 3 shows these stars in the evolutionary context of the CMD. The highest amplitude LPV, V9, is at the extreme giant branch tip, while the low-amplitude LPVs #29 and V24 are situated farther down the giant branch (it is unclear whether any of these LPVs are on the AGB or RGB). The suspected variable #33 is less evolved still, near the variable #38. Our photometry covered only the minimum-light phases of #38, so its position in our CMD is not representative of its actual mean color and magnitude. The suspected variables #7, 14, 26 and 34 lie significantly above the giant branch, suggesting that these centrally-located stars have unresolved stellar blends in our DAOPHOT photometry. Thus, for this moderate-metallicity cluster ([Fe/H] = −1.22, Harris (1996)), pulsation sets in just before the giant branch tip, at $(V - I)_0 = 1.70$, at slightly bluer colors than in the more metal-rich cluster 47 Tucanae (Lebzelter & Wood 2005). None of the stars are cool enough to initiate the large-amplitude pulsations of Mira-type LPVs seen in more metal-rich clusters.

Our photometric study of NGC 1851 has demonstrated that good quality photometry can be done on globular cluster stars down to ∼17 mag using the PROMPT 0.4-m telescopes. Since our data were taken, the pointing, tracking, and collimation of the PROMPT telescopes have been improved, and we expect better results from future images. We have also demonstratd that regular CCD imaging with PROMPT, coupled with modern digital photometric analysis, can clarify and extend the LPV star inventory in globular clusters beyond the existing, largely photographic work. Our time series data indicate that 5-15 day sampling will detect LPVs with amplitudes down to ∼0.1 mag across all but the densest parts of a globular cluster, and produce high quality light curves useful for comparison with stellar pulsation

models (Lebzelter & Wood 2005; Olivier & Wood 2005). We also found that, using the PROMPT #5 telescope, obtaining images in V and I is probably sufficient for future surveys, since B has lower throughput and more scatter in the resulting light curves, and since R provides a narrower color baseline when combined as $V - R$ or $R - I$ compared to $V - I$. We conclude that the PROMPT telescopes and similar robotically-controlled telescopes with moderate pixel scales (0.5-1.0 arcsec) can revive observational work on globular cluster LPVs that has been largely dormant for several decades. Throughout the text, we have described techniques that will be used in our survey of 10-15 predominantly metal-rich globulars using PROMPT.

REFERENCES

Alard, C. 2000, A&AS, 144, 363

Bailey, S. I. 1924, Harvard Bull. 802, 2

Castellani, M., Caputo, F., & Castellani, V. 2003, A&A, 410, 871

Clement, C. M., Muzzin, A., Dufton, Q. et al. 2001, AJ, 122, 2587

Downes, R. A., Margon, B., Homer, L. & Anderson, S. F. 2004, AJ, 128, 2288

Feast, M. W. 1973, IAU Colloq. 21, edited by J. D. Fernie, (Reidel: Dordrecht), 131

Fourcade, C. R. & Laborde, J. R. 1966, Atlas y Catalogo de Estrellas Variables en Cúmulos Globulares al Sur de -29°, Córdoba

Harris, W. E. 1996, AJ, 112, 1487

Layden, A. C. & Sarajedini, A. 2000, AJ, 119, 1760

Lebzelter, T. & Wood, P. R. 2005, A&A, 441, 1117

Liller, M. H. 1975, ApJ, 201, 125

Nemec, J. M., Nemec, A. F. & Lutz, T. E. 1994, AJ, 108, 222

Olivier, E. A. & Wood, P. R. 2005, MNRAS, 362, 1396

Reichart, D., Nysewander, M. Moran, J. et al. 2005, Il Nuovo Cimento C, 28, 767

Stetson, P. B. 1981, AJ, 86 687

Stetson, P. B. 1987, PASP, 99, 191

Stetson, P. B. 1994, PASP, 106, 250

Stetson, P. B. 2000, PASP, 112, 925

Strutskie, M. F. et al. 2006, AJ, 131, 1163

Sumerel, A. N., Corwin, T. M., Catelan, M., Borissova, J., & Smith, H. 2004, IBVS, 5533

Walker, A. R. 1998, AJ, 116, 220

Wehlau, A., Liller, M. H., Demers, S., & Clement, C. C. 1978, AJ, 83, 598

Wehlau, A., Liller, M. H., Clement, C. C. & Wizinowich, P. 1982, AJ, 87, 1295

Zorotovic, M., Catelan, M., Smith, H. A., et al. 2010, AJ, 139, 357
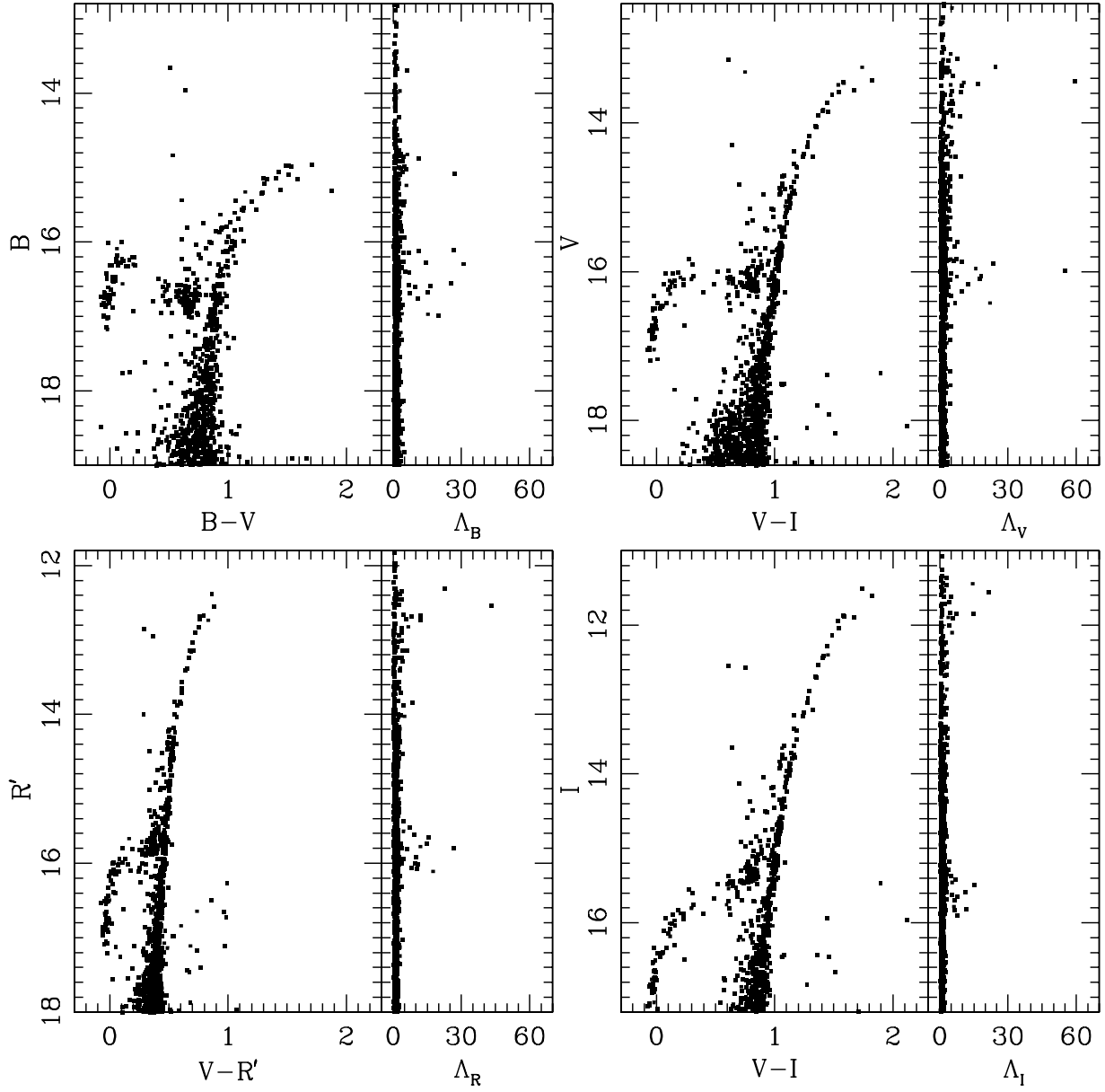
Fig. 1.— Color magnitude diagrams of stars more than 1.0 arcmin from the center of NGC 1851 in different filter combinations. The right-hand panel in each pair plots the variability index in the filter set corresponding to the magnitude used in the left-hand panel; stars at all radial distances are shown in these plots.
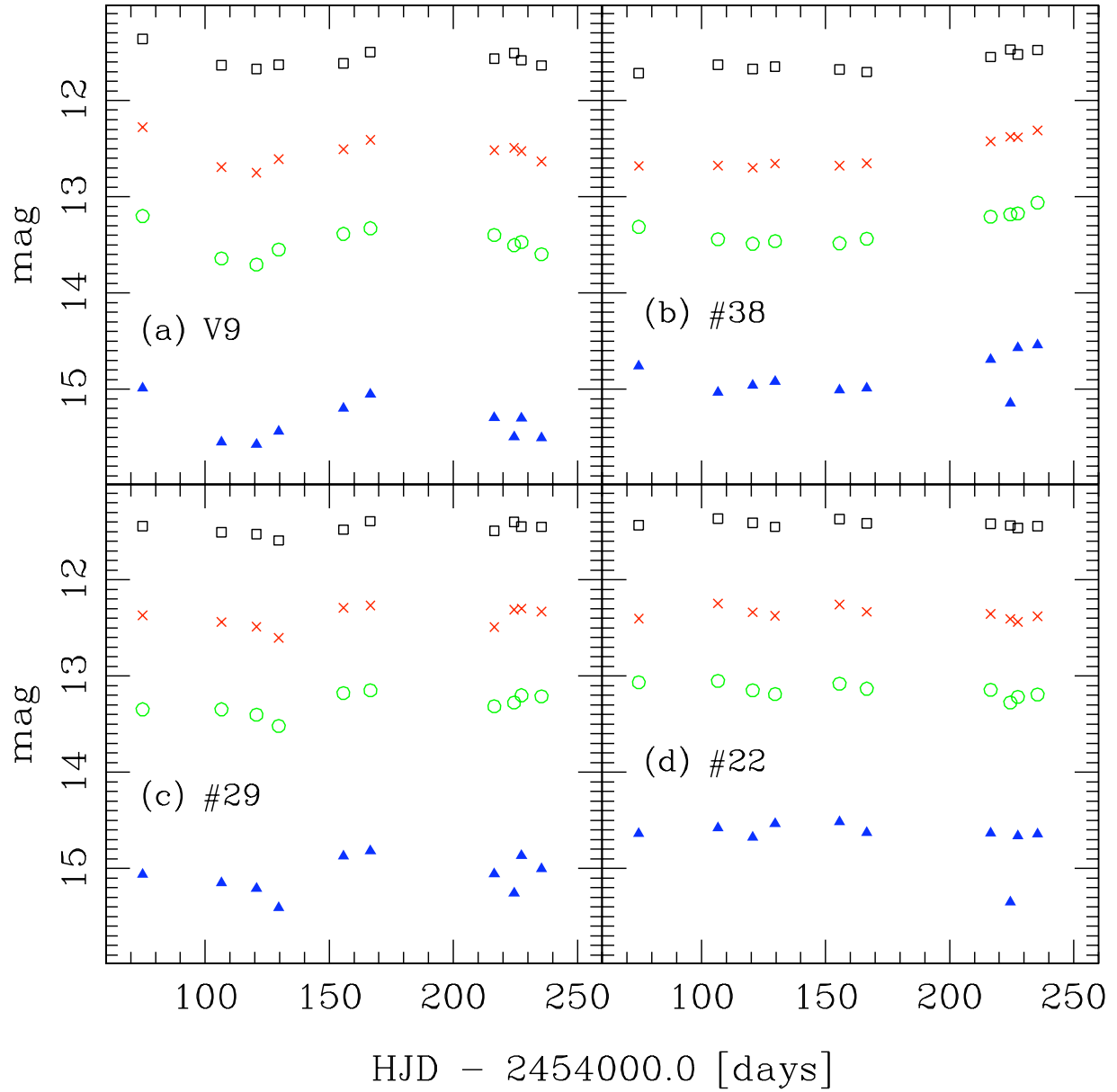
Fig. 2.— Light curves for LPV stars in NGC 1851: (a) V9 = ID#43, (b) ID#38 = new V54, (c) ID#29 = new V55, and (d) the suspected variable ID#22. The light curve magnitudes are coded as B (triangles), V (circles), R' (crosses), and I (squares).
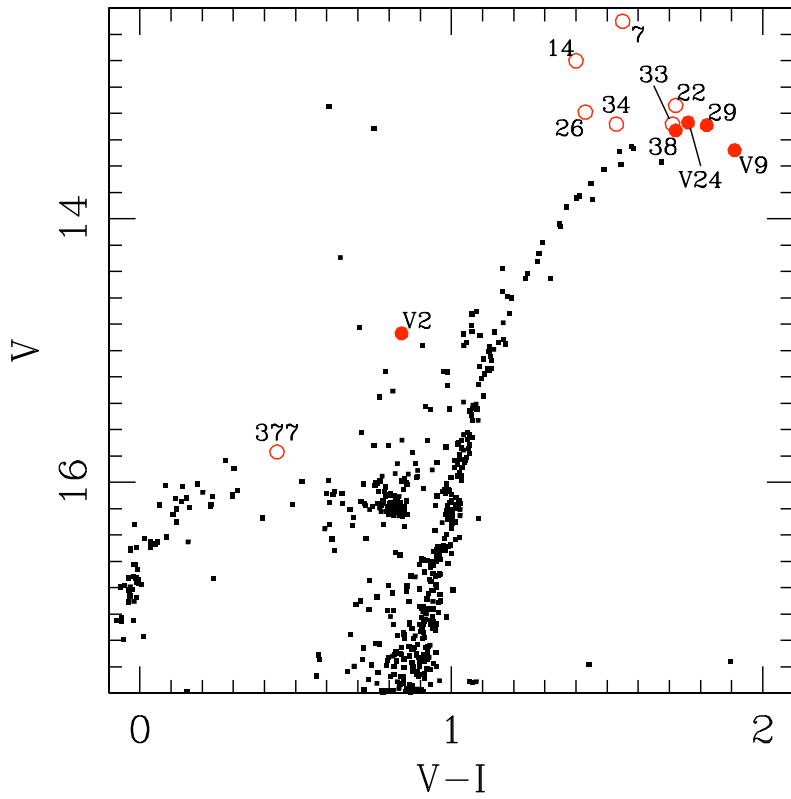
Fig. 3.— The CMD of stars with $R_{proj} > 1.0$ arcmin, with the variable stars (solid circles) and suspected variable stars (open circles) from Table 2 superimposed. The labels indicate the variable star or ID numbers, including our new designations #38 = V54 and #29 = V55.
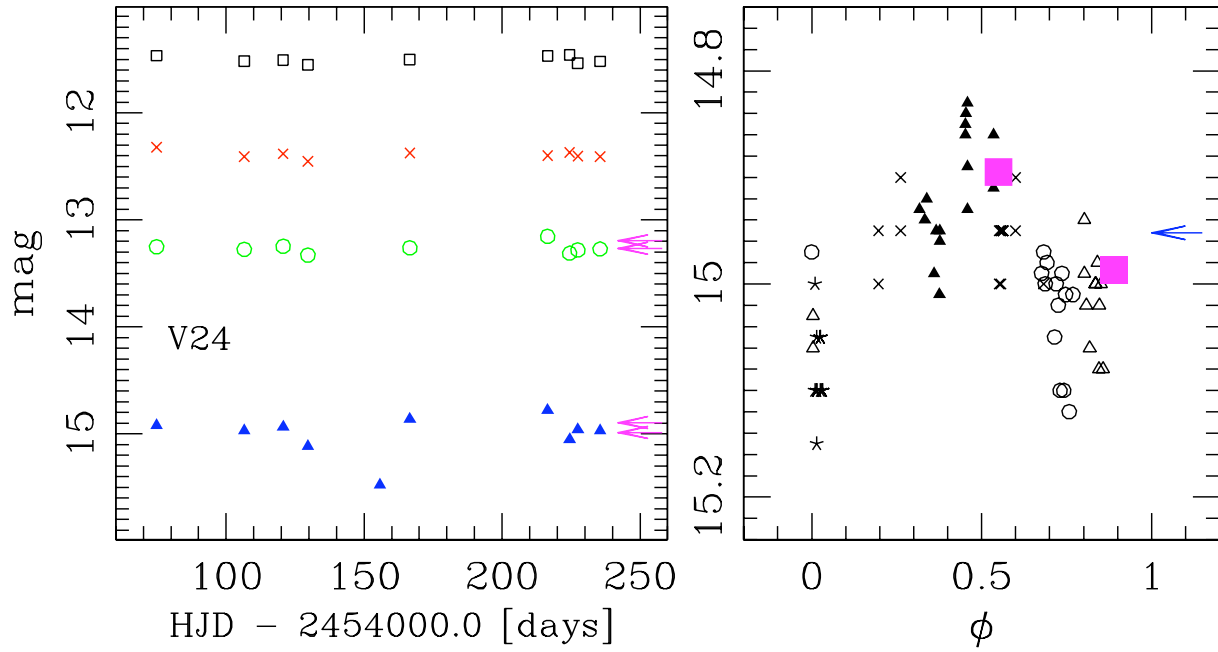
Fig. 4.— The left panel shows our light curves for the LPV star V24 = ID#31 along with arrows indicating the *BV* photoelectric magnitudes of Stetson (1981). In the right panel, the photographic data of Wehlau et al. (1982) are folded with a period of 183 days. These data were acquired during five observing runs: 1972 (circles), 1974/1 (open triangles), 1974/10 (crosses), 1975 (stars), 1980 (filled triangles). The two points from Stetson's (1981) photoelectric photometry, shown as large squares, are correctly phased with the Wehlau data. The mean magnitude of our *B* photometry is shown with an arrow.

Table 1.   Time Series Data of Selected Variable Stars

ID	JD	V	ϵ_V	N_V	B	ϵ_B	N_B	R'	ϵ_R	N_R	I	ϵ_I	N_I	FWHM	Z
43	2,454,074.758	13.201	0.007	10	14.989	0.049	10	12.279	0.103	10	11.359	0.129	10	3.7	1.05
43	2,454,106.634	13.643	0.004	7	15.552	0.003	7	12.691	0.005	7	11.633	0.005	7	2.1	1.02
43	2,454,120.669	13.706	0.002	10	15.576	0.005	10	12.750	0.002	10	11.672	0.005	10	2.6	1.12
43	2,454,129.635	13.549	0.005	9	15.436	0.016	9	12.609	0.005	10	11.628	0.004	10	3.4	1.09
43	2,454,155.673	13.387	0.003	9	15.199	0.008	10	12.507	0.006	8	11.614	0.010	9	2.4	1.70
43	2,454,166.592	13.328	0.006	10	15.052	0.003	10	12.408	0.003	10	11.499	0.001	10	2.8	1.31
43	2,454,216.521	13.398	0.007	10	15.298	0.007	10	12.516	0.006	10	11.566	0.004	10	2.1	1.88
43	2,454,224.487	13.504	0.010	10	15.497	0.040	10	12.492	0.007	10	11.508	0.016	10	3.1	1.73
43	2,454,227.485	13.472	0.006	10	15.300	0.008	10	12.527	0.005	10	11.583	0.005	10	1.9	1.80
43	2,454,235.478	13.598	0.009	10	15.507	0.008	10	12.633	0.007	10	11.636	0.002	10	1.9	2.02
38	2,454,074.758	13.314	0.011	7	14.761	0.069	7	12.680	0.144	7	11.717	0.185	7	3.7	1.05
38	2,454,106.634	13.442	0.005	7	15.031	0.002	7	12.676	0.003	7	11.628	0.006	7	2.1	1.02

Note. — Table 1 is published in its entirety in the electronic edition of the *PASP*. A portion is shown here for guidance regarding its form and content.

Table 2.   Properties of Selected Variable Stars

ID	RA (J2000)	Dec (J2000)	R_{proj}	$\langle V \rangle$	ΔV	$\langle B \rangle$	ΔB	$\langle R' \rangle$	$\Delta R'$	$\langle I \rangle$	ΔI	Comment[a]
43	05:14:01.33	-40:02:05.81	74	13.48	0.5	15.32	0.6	12.54	0.45	11.57	0.3	V9, LPV
38	05:14:09.11	-40:02:54.56	28	13.33	0.45	14.84	0.5	12.54	0.4	11.61	0.2	new V54, BI, LPV
29	05:14:09.70	-40:03:14.72	44	13.29	0.35	15.05	0.6	12.39	0.35	11.47	0.2	new V55, LPV
31	05:14:19.34	-40:04:23.85	173	13.27	0.15	14.96	0.3	12.40	0.1	11.51	0.1	V24, BI, LPV
207	05:14:02.75	-40:02:24.41	51	14.87	0.4	15.52	0.7	14.50	0.25	14.03	0.2	V2=V51, BI, RRab
7	05:14:07.14	-40:02:56.89	11	12.50	0.35	13.80	0.3	11.79	0.3	10.95	0.2	SV, BI
14	05:14:05.81	-40:02:46.03	11	12.80	0.25	14.22	0.4	12.32	0.15	11.40	0.1	SV, BI
22	05:14:07.63	-40:02:26.75	22	13.14	0.15	14.61	0.15	12.35	0.2	11.42	0.1	SV
26	05:14:05.56	-40:03:00.2	19	13.19	0.15	14.48	0.3	12.51	0.1	11.76	0.1	SV, BI
33	05:14:09.19	-40:02:44.01	28	13.28	0.15	14.93	0.25	12.44	0.1	11.57	0.1	SV, BI
34	05:14:09.01	-40:02:46.18	26	13.28	0.1	14.72	0.15	12.54	0.1	11.75	0.1	SV, BI
377	05:14:03.70	-40:03:05.1	39	15.77	0.6	16.08	1.0	15.59	0.6	15.33	0.6	SV, RRL?

[a]BI = blended image, SV = suspected variable.